Continuous flow synthesis of *N,O*-dimethyl-*N'*-nitroisourea monitored by inline FTIR: comparing machine learning and kinetic modeling for optimization

Jiapeng Guo [a], Guihua Luo [a], Kejie Chai [a], Weike Su [a, *], An Su [b, *]

[a] Key Laboratory of Pharmaceutical Engineering of Zhejiang Province, National Engineering Research Center for Process Development of Active Pharmaceutical Ingredients, Collaborative Innovation Center of Yangtze River Delta Region Green Pharmaceuticals, Zhejiang University of Technology, Hangzhou, 310014, P. R. China

[b] State Key Laboratory Breeding Base of Green Chemistry-Synthesis Technology, Key Laboratory of Green Chemistry-Synthesis Technology of Zhejiang Province, College of Chemical Engineering, Zhejiang University of Technology, Hangzhou, Zhejiang 310014, China

***Corresponding Authors:**

Prof. An Su

https://orcid.org/0000-0002-6544-3959

Email: ansu@zjut.edu.cn

Prof. Weike Su

https://orcid.org/0000-0003-2544-1948

Email: pharmlab@zjut.edu.cn

ABSTRACT

The synthesis of *N*,*O*-Dimethyl-*N'*-nitroisourea, crucial intermediates in pesticide manufacturing, was explored through a substitution reaction between *O*-methyl-*N*-nitroisourea and methylamine within a novel continuous flow microreactor system, featuring FTIR inline analysis for real-time monitoring. This study embarked on a comparative analysis between two optimization approaches: the contemporary machine learning-based Bayesian optimization and the traditional kinetic modeling. Remarkably, both strategies obtained a similar yield of approximately 83 % under equivalent reaction parameters---specifically, an initial reactant concentration of 0.2 mol/L, a reaction temperature of 40 °C, a molar ratio of reactants at 5:1, and a residence time of 240 minutes. The Bayesian optimization method demonstrated a notable efficiency, achieving optimal conditions within a mere 20 experiments, in contrast to the kinetic modeling approach, which required a more laborious effort for model formulation and validation. Despite the long-standing reliance on kinetic modeling for its detailed insights into reaction dynamics, our findings suggest its relative inefficiency in optimization tasks compared to the machine learning-based alternative. This study not only highlights the potential of integrating advanced machine learning methods into chemical process optimization but also sets the stage for further exploration into efficient, data-driven approaches in chemical synthesis.

Keywords

Continuous flow; Kinetic modeling; Bayesian optimization; Nucleophilic substitution; FTIR

1. Introduction

N,O-dimethyl-*N*'-nitroisourea (**3**) and 1-methyl-3-nitroguanidine (**4**), crucial intermediates in neonicotinoid insecticides, are produced through the nucleophilic substitution of *O*-methyl-N-nitroisourea (**1**) with methylamine (**2**).[1-5] Traditional methods using batch reactors often struggle with inconsistent reaction conditions and potential safety risks.[6] Continuous flow microreactors have been recognized for their superior mixing efficiency[7,8], precise control over reaction parameters[9], and safety benefits[10-13], showing potential for improving reaction selectivity[14-17]. However, their application in synthesizing these specific intermediates remains unexplored.

Kinetic modeling is a traditional approach to optimizing chemical reactions, deeply rooted in the principles of physical organic chemistry. This approach effectively quantifies the effects of various reaction parameters on conversion and selectivity through mathematical formulas, thus providing direct, actionable guidance for manipulating reaction conditions[18,19]. For example, Su et al. demonstrated the practical application of kinetic modeling to the reaction of m-phenylenediamine and benzoic anhydride. By adjusting key parameters such as initial concentration, reaction temperature, and molar ratio, they fine-tuned the selectivity of the reaction to 96.9 %.[20] Moreover, kinetic models possess the distinct advantage of being extrapolative, enabling the prediction of reaction outcomes beyond the initially explored parameter space, a feature particularly beneficial for scaling up processes.[21] Chamberlain et al. showcased the utility of kinetic modeling in the context of scaling up by studying the aqueous reduction of 4-nitrophenol to 4-aminophenol, facilitated by gold nanoparticles (AuNPs) and sodium borohydride ($NaBH_4$). Their work successfully predicted the optimal conditions for effectively scaling up this reaction.[22] While kinetic modeling has been applied to nucleophilic substitution reactions involving aromatic compounds[23-25], its application to reactions concerning aliphatic compounds remains relatively underexplored.

In recent years, the application of machine learning, particularly Bayesian optimization, has significantly advanced the optimization of continuous flow reactions.[26-29] This method enables the rapid identification of optimal reaction conditions with a minimal number of experiments.[30-33] For instance, Shinichiro et al. utilized Bayesian optimization to efficiently navigate a search space of 10,500 potential reaction condition combinations, successfully identifying the desired conditions for unsymmetrical sulfamide synthesis in just 29 experiments.[34] The efficiency of Bayesian optimization is notably enhanced when integrated with automated platforms. Bourne et al. demonstrated this by developing an automated continuous flow platform for the multistep synthesis of 1-methyltetrahydroisoquinoline C5 functionalization, achieving 81 % of the total yield within 14 hours through Bayesian optimization.[35] Similarly, Doyle et al. applied Bayesian optimization in conjunction with high-throughput screening to optimize multiple reactions, showcasing superior optimization efficiency and consistency compared to traditional human-led decision-making processes.[36] Bayesian optimization uniquely ensures a balance between exploring the chemical space and exploiting the best-known performance conditions.[37,38] Despite its advantages, there remains a scarcity of studies that systematically compare the effectiveness of kinetic modeling and Bayesian optimization in the optimization of continuous flow reactions.

Inline analytical methodologies have markedly enhanced the efficiency of monitoring chemical reactions[39,40], with inline FTIR emerging as a pivotal tool for investigating the kinetics of chemical processes within continuous flow systems[41]. Notably, Jensen et al. have innovated a microfluidic platform that integrates an inline FTIR to accurately quantify reaction conversions while simultaneously characterizing the enthalpy and kinetics of chemical reactions.[42] The non-invasive nature and capability for real-time feedback render inline FTIR an indispensable instrument in the realm of automated synthesis platforms. A recent exemplary study conducted by Jensen and Jamison et al. demonstrates the application of an inline FTIR module within an automated robotic flow platform, facilitating the steady-state monitoring of various reaction phases,

including S_NAr reactions, nitro reductions, and ester activations[43]. This underscores the significant role of inline FTIR in advancing the precision and efficiency of chemical synthesis monitoring.

In this study, we developed a continuous flow microreactor system integrated with an inline FITR designed to optimize the conditions for **1** and **2** nucleophilic substitution reactions. We employed two optimization strategies in parallel: Bayesian optimization and kinetic modeling. The results of these optimization methods were carefully compared to identify their respective strengths and limitations. This comparative analysis reveals the efficacy of each strategy in refining the reaction conditions and provides valuable insights into their applicability in continuous flow chemistry.

2. Materials and methods

2.1 Chemicals

O-methyl-*N*-nitroisourea (**1**, 95 %) Purchased from Qingdao Dexin Chemical Co; Methylamine hydrochloride (**2**, 98.0 %) Purchased from Shanghai Macklin Biochemical Technology Co., Ltd.; $NaHCO_3$ (99 %, Sinopharm Chemical Reagent Co., Ltd.); pure water (AR, Hangzhou Wahaha Group Co., Ltd.); All reagents were used without further purification.

Solution A (**1**): **1** (0.02 mol, 2.382 g) was dissolved in pure water (60 mL), Solution B (**2**+$NaHCO_3$): **2** (0.04 mol, 2.701 g) and $NaHCO_3$ (0.003 mol, 0.252 g) were dissolved in pure water (40 mL).

2.2 Continuous flow microreactor system

The continuous flow microreactor system is shown in Fig. 1. Solutions A and B were stored in two separate syringes (50 mL, Shanghai Kindly Medical Instruments Co., Ltd.) and pumped by two syringe pumps (Pump A, Pump B, ZD-50C6, Suzhou Zede Medical Instrument Co., Ltd.) into the infusion tubing (PTFE, 1/8inch diameter, Wuxi Hongxin

Special Material Technology Co.). The reactants passed through an adapter (PEEK, 1/8inch to 1/16inch, Hangzhou Weimipai Technology Co.) into a sufficiently long (1 m) disk-shaped PTFE capillary tube (PTFE, 1/16inch diameter, Wuxi Hongxin Special Material Technology Co.) to be preheated to the reaction temperature, and mixed in a T-mixer (PEEK, 1/8inch to 1/16inch, Hangzhou Weimipai Technology Co.). The reaction coil (PTFE, 1/8inch diameter) was connected directly to the outlet of the T-mixer. The substitution reaction took place in the reaction coil, and the residence time could be precisely controlled by varying the flow rate of the reaction mixture or the length of the reaction coil. All preheat tubes, T-mixer, and reaction coils were immersed in the same water bath to maintain a constant temperature. Finally, when required the residence time was reached, the reaction was terminated by pumping an excess of purified water through a syringe pump (Pump C, ZD-50C6, Suzhou Zede Medical Instrument Co., Ltd.) into a second T-mixer.

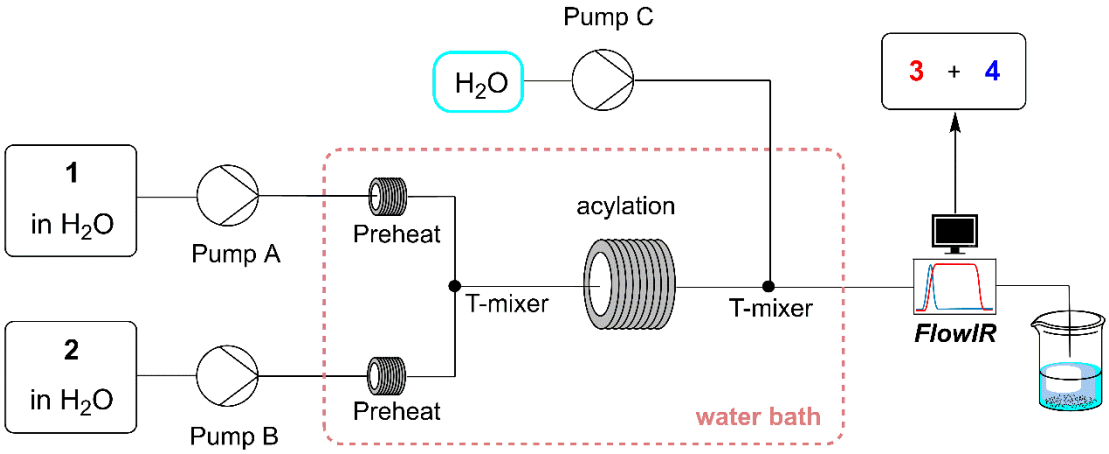

Figure 1. The schematic diagram of the continuous flow microreactor system.

2.3 Sample analysis

When the continuous flow system was operated to a steady state (after 2-3 times the residence time), the reaction solution was quenched and diluted with pure water from the reaction system outlet. The quenched reaction solution was piped into the flow cell for inline infrared detection (METTLER TOLEDO ReactIR ^{TM} 702L) and then flowed to the outlet. Mid-infrared (MIR) band spectra (650-3000 cm^{-1}) were collected by an attenuated total reflection sensor (ATR; diamond, silicon). Because the MIR band

spectra contain diamond absorption bands as well as parts of the concentration-varying infrared with poor correlation to the absorption values, we chased 1048-1582 cm $^{-1}$ band spectra for qualitative and quantitative analyses. (Fig. S1) Quantitative infrared analysis was performed via METTLER TOLEDO iC Quant ^{TM}, each experimental data was repeated three times and averaged, and each measurement consisted of 128 scans. Because of the similar structure of the reactants and products, there were more overlapping IR absorption peaks. We used ConcIRT Live software to build a multivariate analytical model for qualitative and quantitative analysis of the different components. [44]

The reaction order was determined by batch reaction. The reaction solutions were collected for quenching at appropriate times and analyzed by high-performance liquid chromatography (HPLC, ThermoFisher Ulcel3000). The conversion rate of the samples was obtained by constructing the regression equation of the standard curve by the external standard method. HPLC detection conditions C18 column (10 μm, 4.6×250 mm, Welch Materials (Shanghai, China), USA), the mobile phase was 80 % MeOH and 20 % ultrapure water at a flow rate of 1 mL/min, and the detection wavelength was 270 nm. The conversion of **1** was calculated by the following equation:

$$x_{\mathbf{1}} = \left(1 - \frac{C_{\mathbf{1}}}{C_{\mathbf{1}} + C_3 + C_4}\right) \qquad (1)$$

where $x_{\mathbf{1}}$ is the conversion of **1** and C is the molar concentration of the substances in the sample.

The selectivity to **3** was calculated by the following equations:

$$S_3 = \frac{C_3}{C_3 + C_4} \qquad (2)$$

where S is the selectivity to **3**.

The residence time was calculated as follows:

$$t = \frac{V}{Q_1 + Q_2} \qquad (3)$$

where t is the reaction residence time and V is the volume of the microchannel. $Q_{\mathbf{1}}$

and Q_2 are the volume flow rates of the raw material aqueous solution, respectively.

Samples were tested three times under the same conditions and averaged to minimize errors.

2.4. Batch reaction

Batch reactions were carried out using a water bath with magnetic stirring and a single-necked round-bottomed flask (250 ml). This protocol is used only for IR quantitative modeling and determination of the reaction order. Solution A was placed in the single-necked round-bottomed flask with a reaction temperature, Solution B was heated to reaction temperature and poured into the flask quickly all at once. The whole process was carried out under stirring at 850 rpm, it has been proved that the effect of the external diffusion was eliminated. (Fig. S2) Samples were taken periodically during the reaction. The temperature fluctuation during the intermittent reaction is less than 1 °C, and the intermittent reaction can be considered as an isothermal process. Due to the excellent heat transfer performance of the microreactor, the continuous flow reaction is also considered an isothermal process.

3. Results and discussion

In this section, we parallelly perform Bayesian optimization and kinetic modeling for the continuous-flow synthesis of **3** from **1** and **2** (Scheme 1). A comparison of these two optimization methods is then discussed.

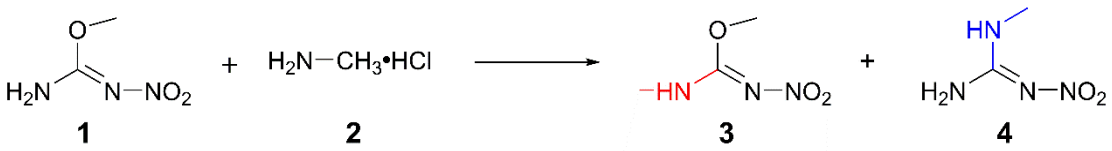

Scheme 1. Synthesis of **3** from **1** and **2**.

3.1 Bayesian optimization

The Bayesian optimization workflow in Fig. 2 begins by defining the search space and

optimization objective. An initial batch of experimental variable values is generated using Latin Hypercube Sample (LHS)[45] and tested in the wet lab. These results train a Gaussian Process (GP) surrogate model. The acquisition function qNEHVI[46] then identifies the next set of variable values for experimentation. This iterative cycle of experimenting with new variable values, updating the dataset, and refining the GP model continues until the predetermined experiment count is met. The optimization was conducted on the FlowBO framework developed in our previous work.[26,47]

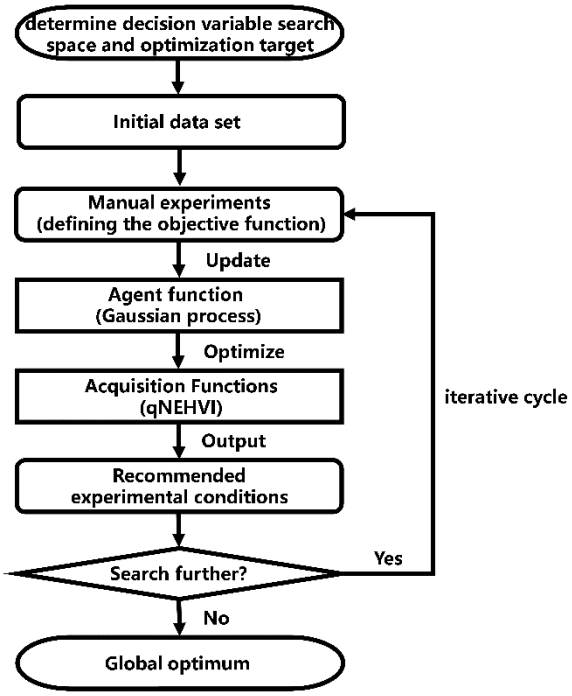

Figure 2. The flowchart of Bayesian optimization in this study.

The optimization objective was defined as maximizing the yield of the principal product **3**. The variable ranges were determined based on the volatility and solubility of the reactants, as well as the measurement capabilities of the ReactIR instrument. Consequently, the reaction temperature was constrained to 20-40 °C, while reactant concentrations were set to 0.05-0.2 mol/L for **1** and 0.04-1 mol/L for **2**. Residence time was limited to a span of 10-240 minutes to simplify the reaction process.

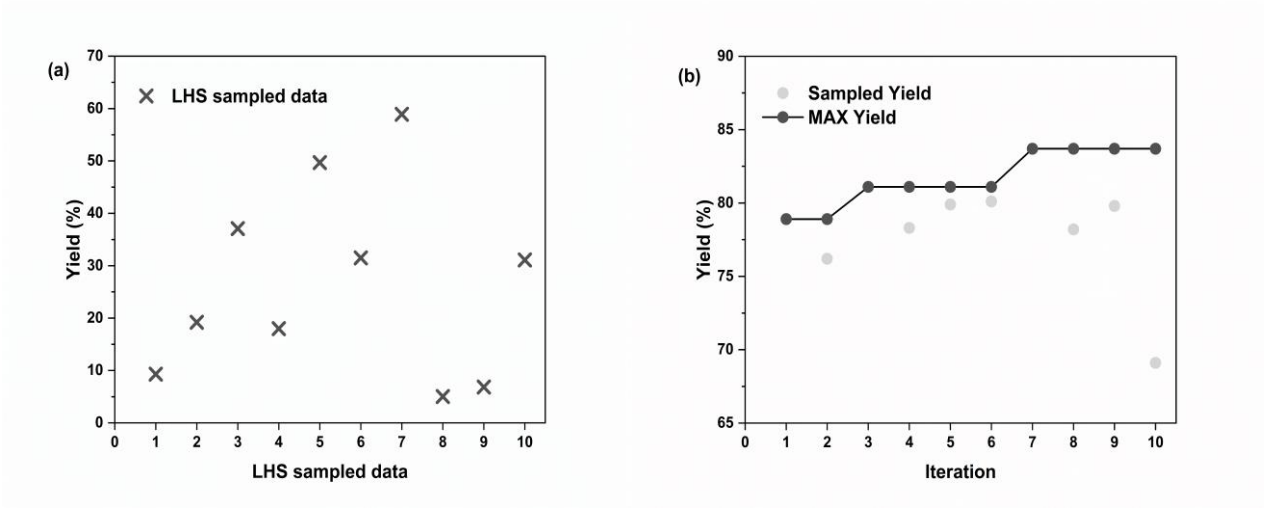

Figure 3. Bayesian optimization results in (a) LHS sampling stage and (b) optimization stage.

Fig. 3 shows the yield of **3** under the experimental variables sampled by the LHS stage (a) and the optimization stage (b). After ten experiments, an optimized yield of 83.7 % was found from the 7th iteration of the optimization stage. The corresponding values of reaction variables are shown in Table 1. We found that the model not only exploits around the current optimum but also explores the high-uncertainty areas even if they are distant from the current optimum, which escaped the optimization from falling into a local optimum.

Table 1. Iterative optimization data and results.

Data type	Entry	Time (min)	Temp (°C)	**1** (mol/L)	**2** Molar ratio	Yield (%)
LHS sampled data	1	205	21.0	0.0575	2.27	0.093
	2	67.5	37.0	0.163	1.43	0.192
	3	114	27.0	0.118	4.79	0.371
	4	44.5	39.0	0.0725	3.53	0.180
	5	228	35.0	0.0875	3.11	0.497
	6	136	29.0	0.132	2.69	0.315
	7	159	31.0	0.192	3.95	0.589

	8	21.5	33.0	0.147	1.85	0.0503
	9	182	25.0	0.102	1.01	0.0684
	10	90.5	23.0	0.177	4.37	0.311
-Acquisition function suggested data	1	240	35.5	0.168	4.63	0.789
	2	240	35.1	0.200	3.56	0.762
	3	200	40.0	0.200	4.31	0.811
	4	240	40.0	0.164	3.34	0.783
	5	194	40.0	0.154	5.00	0.799
	6	240	40.0	0.112	5.00	0.801
	7	240	40.0	0.200	5.00	0.837
	8	124	40.0	0.200	5.00	0.782
	9	240	32.5	0.200	5.00	0.798
	10	240	40.0	0.200	2.04	0.691

(During the experiment, we rounded some of the parameters due to the limited precision of the instrument.)

3.2 Kinetic modeling and optimization using the kinetic model

The workflow of kinetic modeling is shown in Fig. 4.

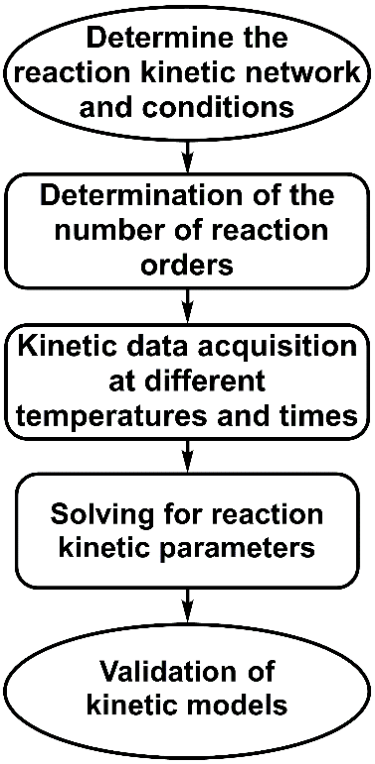

Figure 4. The workflow of kinetic modeling in this study.

Initial screening experiments established the experimental conditions of kinetic modeling, setting the maximum concentration of the stock solution of **1** at 0.4 mol/L to avoid precipitation based on its solubility of 0.5 mol/L in water at 20 °C. The molar ratio of **2** to **1** was 2: 1 as no further improvements in the conversion of **1** or the selectivity of **3** were observed beyond this ratio (Fig. S3). The liquid flow rate was set at 5 ml/h since lower rates significantly reduced the conversion of **1**.

The reaction orders for **1** and **2** were determined using a batch reactor (Fig. S4). The initial concentration of **2** was five times that of **1**, resulting in an excessive presence of **2**. Consequently, eq. 4 was reformulated to depend on α (the reaction order of **1)** and the apparent rate constant K_{β}. The reaction time and conversion were correlated with first-order (eq. 5) and second-order (eq. 6) reaction laws. The results of these fittings are in Fig. 5a for the first-order reaction and Fig. 5b for the second-order reaction. The higher R^2 value observed in Fig. 5a confirms that the reaction order for **1** is indeed first-

order.

$$-\frac{dC_1}{dt} = kC_1{}^{\alpha}C_2{}^{\beta} \approx K_{\beta}C_1{}^{\alpha} \quad (4)$$

$$ln(1 - x_1) = -K_{\beta}t \quad (5)$$

$$\frac{1}{1-x_1} = 1\text{-}K_{\beta}t \quad (6)$$

Where k is the rate constant for the consumption of **1**, C_1 and C_2 are the concentrations of **1** and **2**, α and β are reaction orders of **1** and **2,** K_{β} is the apparent reaction rate constant when **2** is excessive, x_1 = 1- C_1/C_{10} where C_{10} is the initial concentration of **1**, and t is the reaction time in the batch reactor.

Given the reaction order of **1** was first-order, eq. 4 was transformed into eq. 7. Considering that a total reaction order exceeding two is uncommon for bimolecular reactions, we limited our investigation to scenarios where the reaction order of **2**, denoted as β, could be 0 or 1. This was done by fitting the reaction data to eq. 8 and 9. The R^2 of 0.997 for the first-order assumption (Fig. 5d) surpasses the R^2 of 0.988 for the second-order assumption (Fig. 5c). Therefore, the reaction order for **2** was also first-order.

$$-\frac{dC_1}{dt} = kC_1C_2{}^{\beta} \quad (7)$$

$$ln(1 - x_1) = -kt \quad (8)$$

$$\frac{1}{C_{20}-C_{10}} ln\left(\frac{1-x_2}{1-x_1}\right) = -kt \quad (9)$$

where k is the rate constant for the consumption of **1**, C_1 and C_2 are the concentrations of **1** and **2**, β is the reaction order of **2,** C_{10} and C_{20} are the initial concentrations of **1** and **2,** x_1 = 1- C_1/C_{10}, x_2 = 1- C_2/C_{20}, and t is the reaction time in the batch reactor.

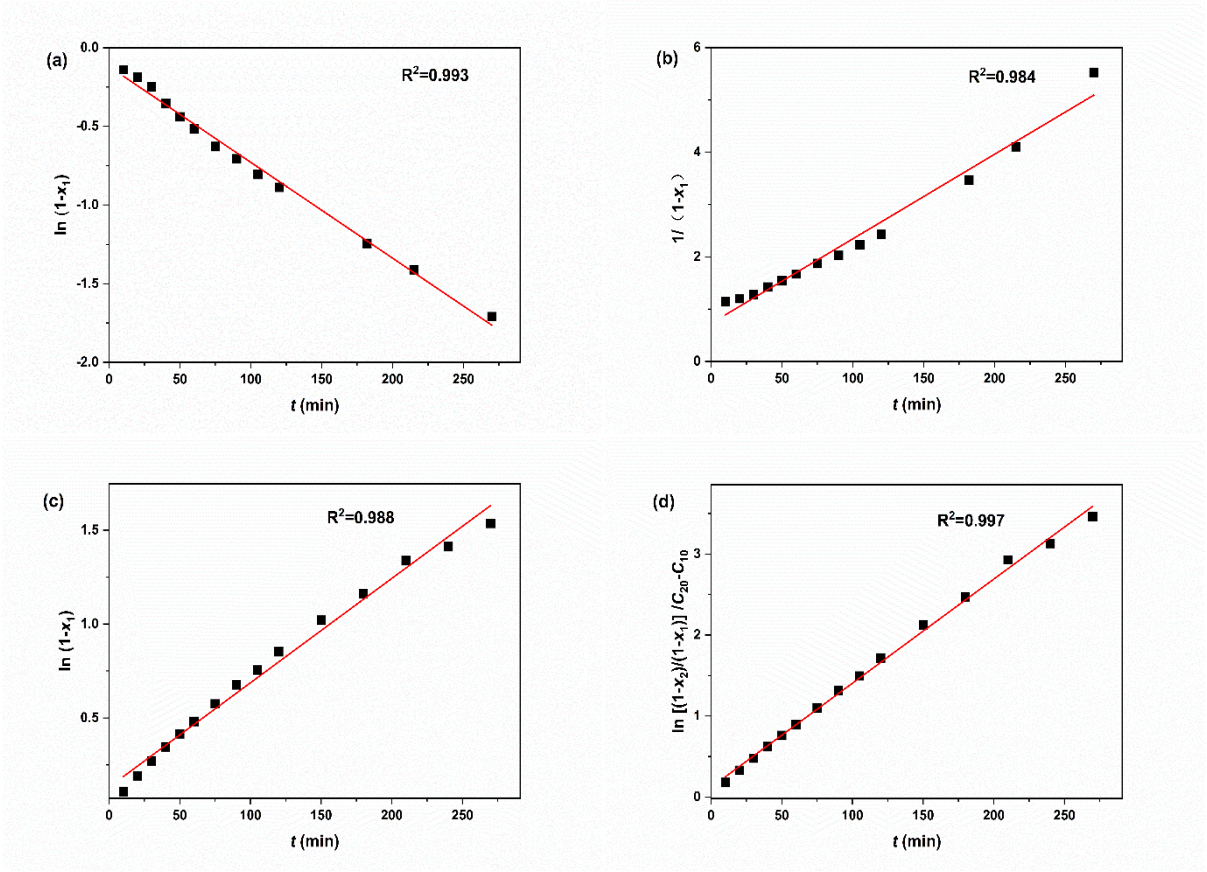

Figure 5. Determination of the reaction orders for **1** (a). $\ln(1-x_1)$ versus *t*; (b). $\frac{1}{1-x_1}$ versus *t*; and **2** (c) $\ln(1-x_1)$ versus *t*; (d). $\frac{1}{C_{20}-C_{10}}\ln\left(\frac{1-x_2}{1-x_1}\right)$ versus *t*. Determination of **1** reaction order conditions: reaction temperature (T) = 30 °C; initial concentration of reactants in reaction mixture: C_{10} = 0.2 mol/L, C_{20} = 1 mol/L and C_{NaHCO_3} = 0.03 mol/L; stirring speed = 850 rpm. Determination of **2** reaction order conditions: reaction temperature (T) = 30 °C; initial concentration of reactants in reaction mixture: C_{10} = 0.3 mol/L, C_{20} = 0.6 mol/L, C_{NaHCO_3} = 0.045 mol/L; stirring speed = 850 rpm.

With the reaction order determined, the following experiments were performed in a continuous flow reactor. Eq. 9 was reformulated as eq. 10.

$$ln\left[\frac{M-x_1}{M(1-x_1)}\right] = K\tau \qquad (10)$$

where $M = C_{20}/C_{10}$ and $K = (M\text{-}1)\ C_{10}k$, C_{10} and C_{20} are the initial concentrations of **1** and **2,** $x_1 = 1\text{-}\ C_1/C_{10}$, and τ is the residence time in the continuous flow reactor.

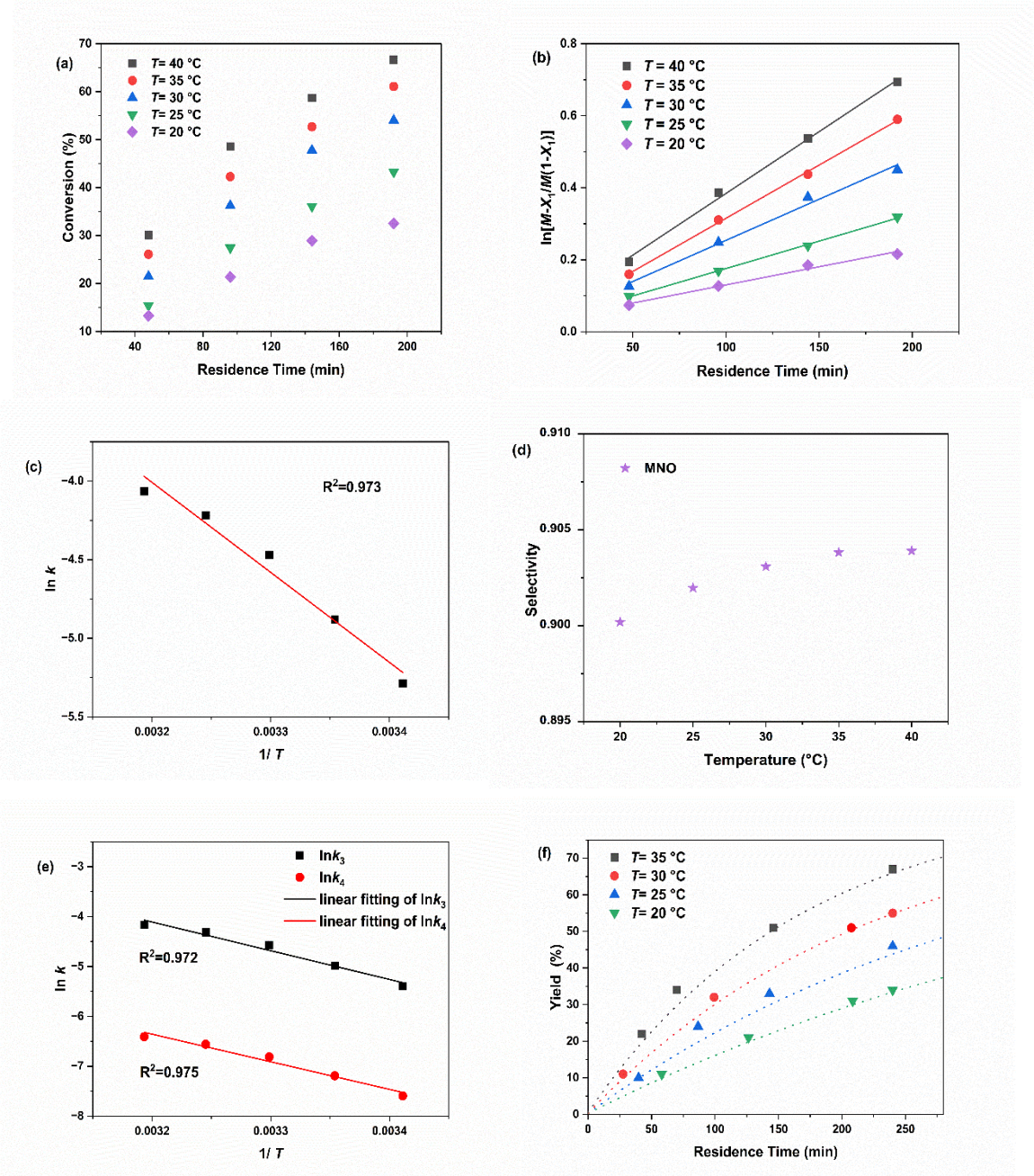

Figure 6. (a). The conversion of **1** at different temperatures and residence times. (b). Determination of *K* at different temperatures. (c). Arrhenius plot of ln *k* versus 1/*T*. (d). The conversion of **4** at different temperatures and residence times. (e). Arrhenius plots of ln *k versus* 1/*T* for forming **3** and **4**. (f). Comparison of the experimental (data points) and predicted (dotted lines) values for **3** yield at different temperatures. Collection of kinetic data reaction conditions: initial concentration of reactants in reaction mixture: C_{10} = 0.2 mol/L, C_{20} = 0.4 mol/L, C_{NaHCO_3} = 0.03 mol/L; the flow rate: Solution A (Q_A) = 3 mL/h, Solution B (Q_B) = 2 mL/h, quenched H_2O solution C(Q_C) = 100 mL/h; the residence time was controlled by changing the length of reacting tubes. The reaction conversion rate and yield is monitored in real time by inline infrared.

Fig. 6a displays the temperature-dependent conversion of **1** with residence time. The

rate constants (k) at varying temperatures were determined by fitting eq. 10, with all fits showing R^2 values above 0.99 (Fig. 6b). The activation energy Ea and pre-exponential factor A were calculated from these k values using the Arrhenius equation (eq. 11). The Arrhenius plot of ln k versus $1/T$ is depicted in Fig. 6c, from which Ea and ln A were obtained (Table 1).

$$ln\,k = ln\,A - \frac{E_a}{RT} \qquad (11)$$

where k is the rate constant, Ea is the activation energy, A is the pre-exponential factor, R is the molar gas constant, and T denotes the Kelvin temperature.

Assuming that the production of **3** and **4** occurs via competitive parallel pathways, each adhering to identical reaction kinetics but with distinct rate constants, the overall reaction rate constant k can be disaggregated into k_3 and k_4 for **3** and **4**, respectively, as delineated in eq. 12. Consequently, the selectivity towards **3** (S_3) can be described by eq. 13**:**

$$k = k_3 + k_4 \qquad (12)$$

$$S_3 = \frac{k_3 C_1 C_2}{k_3 C_1 C_2 + k_4 C_1 C_2} = \frac{k_3}{k_3 + k_4} = \frac{k_3}{k} \qquad (13)$$

where k is the overall rate constant, k_3 and k_4 are rate constant for the production of **3** and **4**, S_3 is the selectivity of **3**, and C_1 and C_2 are the concentrations of **1** and **2**.

Our observations indicate that the selectivity towards **3** remains unaffected by the residence time (Fig. S5). Therefore, the selectivity of **3** at varying temperatures was investigated (Fig. 6d). Utilizing these data, the corresponding values of k_3 and k_4 were computed according to eq. 13. The activation energies (Ea$_3$, Ea$_4$) and pre-exponential factors for the concurrent synthesis of **3** and **4** were determined in the same way as in eq. 11 (Fig. 6e) and the corresponding values of these constants are presented in Table 2.

Table 2. Values of the pre-exponential factors and activation energies of the overall reaction and two parallel reactions

Factors	Ea (J/mol)	ln A	Ea$_3$ (J/mol)	ln A_3	Ea$_4$ (J/mol)	ln A_4

Values	47,605.33	14.31	47,786.04	14.28	45,939.65	11.33

A series of validation experiments were conducted with a temperature range of 20-35 °C and a residence time of 27-240 min (Fig. 6f). The yields of **3** predicted from the kinetic model were in good agreement with the experimental data, thereby confirming the validity of the kinetic model. With the kinetic model constructed, we plot the response surface at three different levels of molar ratio (Fig. 7). High temperature is more favorable for the formation of **3** since Ea_3 is higher than Ea_4. In addition, higher molar ratio and reaction time are also preferred for a higher yield. Therefore, the optimized reaction conditions for **3** were obtained by kinetic modeling: the initial concentration of **1** was 0.2 mol/L, the reaction temperature was 40 °C, the molar ratio was 5:1, and the reaction time was 240 min. The yield predicted by the kinetic models under these conditions was 96.4 %, while the experimentally measured yield under the same condition was 82.9 %.

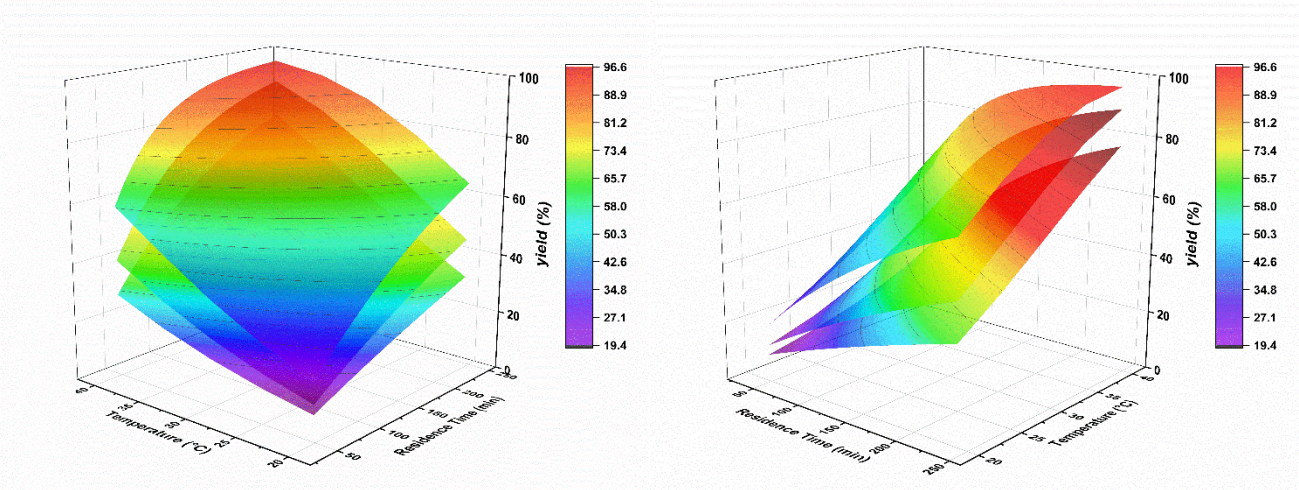

Figure 7. The response surfaces of kinetic modeling from two perspectives. The molar ratio of the surfaces from top to bottom are 5:1, 3:1, and 2:1

3.3 Comparison of kinetic modeling with Bayesian optimization results

In terms of optimization, the kinetic model, while comprehensive, is less efficient than the Bayesian optimization. Constructing a kinetic model involved a multi-step

experimental process: 5 experiments were performed to determine the range of variables that minimize non-chemical kinetic phenomena. This was followed by 7 experiments to determine the reaction orders and 20 experiments to calculate the key parameters such as rate constants, activation energies, and pre-exponential factors. A further 16 experiments were required to validate the kinetic model. Subsequently, reaction surfaces were generated, and optimal reaction conditions were determined at the peak points of these surfaces.

Furthermore, the predictive accuracy of the kinetic model's yield decreased when variables exceeded the range used for its construction. This discrepancy was highlighted in Fig. 8, where actual yields did not match the model's predictions. For example, a yield predicted to be 82.0 % under conditions of 468 minutes at 35 °C was actually 77.1 %, and a yield forecasted at 55.3 % for 506 minutes at 25 °C ended up being 49.8 %. This issue likely stems from the model's dependence on experimental data, which may inherently contain errors. As the explored variables move beyond the bounds of the initial experimental data, these errors can accumulate, affecting the model's reliability. Despite these discrepancies in yield predictions, it is noteworthy that such deviations did not affect the identification of optimal reaction conditions.

Conversely, Bayesian optimization demonstrated a more streamlined approach, achieving the same optimal results as kinetic modeling within only 20 experiments. One of the significant advantages of Bayesian optimization is its elimination of the validation step required in kinetic modeling. This is because the surrogate model in Bayesian optimization is utilized solely for suggesting potential reaction conditions rather than predicting the outcomes of reactions. As a result, all findings obtained through Bayesian optimization are directly determined through experimental means. This comparison highlights the efficiency and practicality of Bayesian optimization in optimizing chemical reactions, suggesting it is a preferable method when rapid and reliable results are paramount.

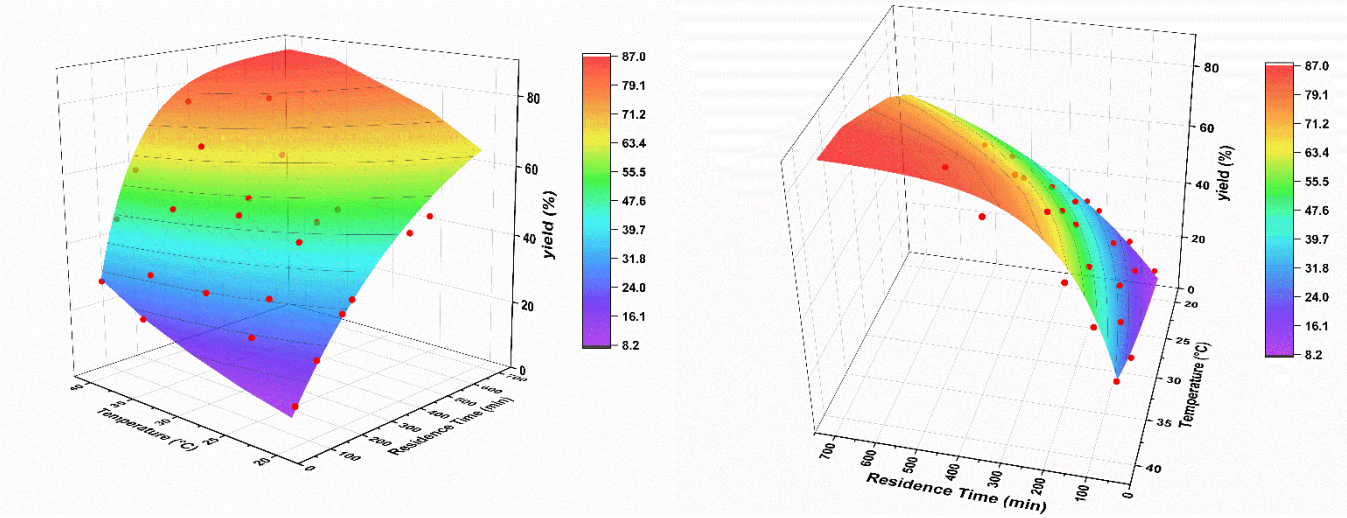

Figure 8. Comparison of response surface predicted by kinetic model and the experimentally determined values (red dots).

4. Conclusion

In this study, we developed a continuous flow microfluidic system equipped with FTIR inline analysis for the monosubstitution reactions of *O*-methyl-*N*-nitroisourea and methylamine. The effectiveness of machine learning-based Bayesian optimization and kinetic modeling in optimizing this reaction was compared. Bayesian optimization obtained optimized reaction conditions and a main-product yield of 83.7 % within only 20 experiments. In contrast, kinetic modeling required a significantly larger experimental effort to reach similar optimal conditions and yield. Despite kinetic modeling's traditional advantage in providing a detailed description of the reaction space, it proved less efficient for optimization purposes. Moreover, kinetic modeling faced challenges in accuracy when reaction variables extended beyond the initial model construction space, highlighting a need for additional data to improve yield estimations.

Declaration of Competing Interest

The authors declare that they have no known competing financial interests or personal relationships that could have appeared to influence the work reported in this paper.

Acknowledgments

This research was supported by the Joint Funds of the Zhejiang Provincial Natural Science Foundation of China under Grant No. LHDMZ23B060001, Zhejiang Province Science and Technology Plan Project under Grant No. 2022C01179, and the National Natural Science Foundation of China under Grant No. 22108252.

Appendix A. Supplementary data

Supplementary data to this article can be found online at XXXXXXXXXXXXXX.

References

(1) Uneme, H.; Kamiya, Y.; Konobe, M.; Yamada, J. Manufacture of *N*-(heterocyclylmethyl)-*N'*-nitroisoureas. WO9933809A1, 1999.

(2) Matsuno, H.; Arai, K.; Oura, T.; Kodaka, K. Preparation of nitroisoureas as intermediates for nitroguanidine insecticides. EP974579A1, 2000.

(3) Maienfisch, P.; Huerlimann, H.; Haettenschwiler, J. A novel method for the preparation of *N,N'*-disubstituted *N''*-nitroguanidines, including a practical synthesis of the neonicotinoid insecticide clothianidin. *Tetrahedron Lett.* **2000**, *41* (37), 7187-7191.

(4) Kamekawa, H.; Miyashita, T.; Katsuta, H.; Kitashima, T. Improved method for producing nitroguanidine derivative. WO2007091391A1, 2007.

(5) Wang, Q.; Wu, Y.; Wang, K.; Sun, Y.; Zhu, H.; Yu, J.; Xu, C. Process improvements for the preparation of insecticide clothianidin. *Asian Journal of Chemistry* **2014**, *26* (10), 2815-2819.

(6) Copelli, S.; Barozzi, M.; Maestri, F.; Rota, R. Safe optimization of potentially runaway reactions: From fedbatch to continuous stirred tank type reactor. *Journal of Loss Prevention in the Process Industries* **2018**, *55*, 289-302.

(7) Yoshida, J. I.; Kim, H.; Nagaki, A. Green and Sustainable Chemical Synthesis Using Flow Microreactors. *Chemsuschem* **2011**, *4* (3), 331-340.

(8) Schwalbe, T.; Autze, V.; Hohmann, M.; Stirner, W. Novel Innovation Systems for a Cellular Approach to Continuous Process Chemistry from Discovery to Market. *Organic Process Research & Development* **2004**, *8* (3), 440-454.

(9) Neyt, N. C.; Riley, D. L. Application of reactor engineering concepts in continuous flow chemistry: a review. *Reaction Chemistry & Engineering* **2021**, *6* (8), 1295-1326.

(10) Köckinger, M.; Wyler, B.; Aellig, C.; Roberge, D. M.; Hone, C. A.; Kappe, C. O. Optimization and Scale-Up of the Continuous Flow Acetylation and Nitration of 4-Fluoro-2-methoxyaniline to Prepare a Key Building Block of Osimertinib. *Organic Process Research & Development* **2020**, *24* (10), 2217-2227.

(11) Kockmann, N.; Thenée, P.; Fleischer-Trebes, C.; Laudadio, G.; Noël, T. Safety assessment in development and operation of modular continuous-flow processes. *Reaction Chemistry & Engineering* **2017**, *2* (3), 258-280.

(12) Du, C.; Hu, Y.; Zhang, J.; Luo, G. Ultra-low formation of octahydrophenazine in the Beckmann

rearrangement of cyclohexanone oxime using a microreactor. *Reaction Chemistry & Engineering* **2019**, *4* (11), 1991-1999.
(13) Yan, Z.; Ma, Z.; Deng, J.; Luo, G. Mechanism and kinetics of epoxide ring-opening with carboxylic acids catalyzed by the corresponding carboxylates. *Chemical Engineering Science* **2021**, *242*, 116746.
(14) Bukhtiyarova, M. V.; Nuzhdin, A. L.; Bukhtiyarova, G. A. Comparative Study of Batch and Continuous Flow Reactors in Selective Hydrogenation of Functional Groups in Organic Compounds: What Is More Effective? *International Journal of Molecular Sciences* **2023**, *24* (18), 14136.
(15) Naik, P.; Garcia-Lacuna, J.; Oneill, P.; Baumann, M. Continuous Flow Oxidation of Alcohols Using TEMPO/NaOCl for the Selective and Scalable Synthesis of Aldehydes. *Organic Process Research & Development* **2023**, Ahead of Print.
(16) Mouhsine, B.; Saint Pol, A.; Karim, A.; Penhoat, M.; Dumont, C.; Suisse, I.; Sauthier, M. Sustainable and selective Ni-catalyzed allylation of 2-oxindoles and 2-coumaranones in batch and flow chemistry. *Reaction Chemistry & Engineering* **2023**, *8* (10), 2549-2556.
(17) Xie, X.; Xie, S.; Yao, H.; Ye, X.; Yu, Z.; Su, W. Green and catalyst-free synthesis of deoxyarbutin in continuous-flow. *Reaction Chemistry & Engineering* **2019**, *4* (5), 927-931.
(18) Willis, M. J.; Stosch, M. v. Inference of chemical reaction networks using mixed integer linear programming. *Computers & Chemical Engineering* **2016**, *90*, 31-43.
(19) Taylor, C. J.; Pomberger, A.; Felton, K. C.; Grainger, R.; Barecka, M.; Chamberlain, T. W.; Bourne, R. A.; Johnson, C. N.; Lapkin, A. A. A Brief Introduction to Chemical Reaction Optimization. *Chemical Reviews* **2023**, *123* (6), 3089-3126.
(20) Xu, Q.; Fan, H.; Yao, H.; Wang, D.; Yu, H.; Chen, B.; Yu, Z.; Su, W. Understanding monoacylation of symmetrical diamines: A kinetic study of acylation reaction of *m*-phenylenediamine and benzoic anhydride in microreactor. *Chemical Engineering Journal* **2020**, *398*, 125584.
(21) Wagner, F.; Sagmeister, P.; Jusner, C. E.; Tampone, T. G.; Manee, V.; Buono, F. G.; Williams, J. D.; Kappe, C. O. A Slug Flow Platform with Multiple Process Analytics Facilitates Flexible Reaction Optimization. *n/a* (n/a), 2308034.
(22) Hall, B. L.; Taylor, C. J.; Labes, R.; Massey, A. F.; Menzel, R.; Bourne, R. A.; Chamberlain, T. W. Autonomous optimisation of a nanoparticle catalysed reduction reaction in continuous flow. *Chemical Communications* **2021**, *57* (40), 4926-4929.
(23) Asghar, B. H. Kinetic study of nucleophilic reactivity of heterocyclic amines with 4,6-dinitrobenzofuroxan in acetonitrile. *Arabian Journal of Chemistry* **2019**, *12* (8), 2476-2483.
(24) Hsu, H.-L.; Yang, C.-C.; Chiu, W.-C.; Hou, S.-S.; Lin, C.-Y.; Lin, C.-L. Kinetic model, recycling, regeneration, and reusing of tri-phase catalytic nucleophilic substitution esterification. *Molecular Catalysis* **2022**, *531*, 112657.
(25) Bhargavi, K.; Shyamala, P.; Padma, M.; Nagalakshmi, K. V. Kinetic study of S_N2 reaction between paranitrophenyl benzoate and hydrazine in the presence of CTAB reverse micelles. *Bulletin of Chemical Reaction Engineering and Catalysis* **2021**, *16* (4), 744-751.
(26) Qi, T.; Luo, G.; Xue, H.; Su, F.; Chen, J.; Su, W.; Wu, K.-J.; Su, A. Continuous heterogeneous synthesis of hexafluoroacetone and its machine learning-assisted optimization. *Journal of Flow Chemistry* **2023**, *13* (3), 337-346.
(27) Karan, D.; Chen, G.; Jose, N.; Bai, J.; McDaid, P.; Lapkin, A. A. A machine learning-enabled process optimization of ultra-fast flow chemistry with multiple reaction metrics. *React. Chem. Eng.*

2023, Ahead of Print.
(28) Taylor, C. J.; Felton, K. C.; Wigh, D.; Jeraal, M. I.; Grainger, R.; Chessari, G.; Johnson, C. N.; Lapkin, A. A. Accelerated chemical reaction optimization using multi-task learning. *ChemRxiv* **2023**, 1-41.
(29) Kershaw, O. J.; Clayton, A. D.; Manson, J. A.; Barthelme, A.; Pavey, J.; Peach, P.; Mustakis, J.; Howard, R. M.; Chamberlain, T. W.; Warren, N. J.; Bourne, R. A. Machine learning directed multi-objective optimization of mixed variable chemical systems. *Chem. Eng. J. (Amsterdam, Neth.)* **2023**, *451* (Part_1), 138443.
(30) Clayton, A. D.; Manson, J. A.; Taylor, C. J.; Chamberlain, T. W.; Taylor, B. A.; Clemens, G.; Bourne, R. A. Algorithms for the self-optimisation of chemical reactions. *Reaction Chemistry & Engineering* **2019**, *4* (9), 1545-1554.
(31) Sagmeister, P.; Ort, F. F.; Jusner, C. E.; Hebrault, D.; Tampone, T.; Buono, F. G.; Williams, J. D.; Kappe, C. O. Autonomous Multi-Step and Multi-Objective Optimization Facilitated by Real-Time Process Analytics. *Advanced Science* **2022**, *9* (10), 2105547.
(32) Zhang, J.; Sugisawa, N.; Felton, K. C.; Fuse, S.; Lapkin, A. A. Multi-objective Bayesian optimisation using q-noisy expected hypervolume improvement (qNEHVI) for the Schotten-Baumann reaction. *React. Chem. Eng.* **2023**, Ahead of Print.
(33) Jorayev, P.; Russo, D.; Tibbetts, J. D.; Schweidtmann, A. M.; Deutsch, P.; Bull, S. D.; Lapkin, A. A. Multi-objective Bayesian optimisation of a two-step synthesis of *p*-cymene from crude sulphate turpentine. *Chemical Engineering Science* **2022**, *247*, 116938.
(34) Sugisawa, N.; Sugisawa, H.; Otake, Y.; Krems, R. V.; Nakamura, H.; Fuse, S. Rapid and Mild One-Flow Synthetic Approach to Unsymmetrical Sulfamides Guided by Bayesian Optimization. **2021**, *1* (11), 484-490.
(35) Clayton, A. D.; Pyzer-Knapp, E. O.; Purdie, M.; Jones, M. F.; Barthelme, A.; Pavey, J.; Kapur, N.; Chamberlain, T. W.; Blacker, A. J.; Bourne, R. A. Bayesian Self-Optimization for Telescoped Continuous Flow Synthesis. *Angew. Chem., Int. Ed.* **2023**, *62* (3), e202214511.
(36) Shields, B. J.; Stevens, J.; Li, J.; Parasram, M.; Damani, F.; Alvarado, J. I. M.; Janey, J. M.; Adams, R. P.; Doyle, A. G. Bayesian reaction optimization as a tool for chemical synthesis. *Nature* **2021**, *590* (7844), 89-96.
(37) Shahriari, B.; Swersky, K.; Wang, Z.; Adams, R. P.; Freitas, N. d. Taking the Human Out of the Loop: A Review of Bayesian Optimization. *Proceedings of the IEEE* **2016**, *104* (1), 148-175.
(38) Bradford, E.; Schweidtmann, A. M.; Lapkin, A. Efficient multiobjective optimization employing Gaussian processes, spectral sampling and a genetic algorithm. *Journal of Global Optimization* **2018**, *71* (2), 407-438.
(39) Sagmeister, P.; Lebl, R.; Castillo, I.; Rehrl, J.; Kruisz, J.; Sipek, M.; Horn, M.; Sacher, S.; Cantillo, D.; Williams, J. D.; Kappe, C. O. Advanced Real-Time Process Analytics for Multistep Synthesis in Continuous Flow**. **2021**, *60* (15), 8139-8148.
(40) Cortés-Borda, D.; Wimmer, E.; Gouilleux, B.; Barré, E.; Oger, N.; Goulamaly, L.; Peault, L.; Charrier, B.; Truchet, C.; Giraudeau, P.; Rodriguez-Zubiri, M.; Le Grognec, E.; Felpin, F.-X. An Autonomous Self-Optimizing Flow Reactor for the Synthesis of Natural Product Carpanone. *The Journal of Organic Chemistry* **2018**, *83* (23), 14286-14299.
(41) Fath, V.; Lau, P.; Greve, C.; Kockmann, N.; Röder, T. Efficient Kinetic Data Acquisition and Model Prediction: Continuous Flow Microreactors, Inline Fourier Transform Infrared Spectroscopy, and Self-Modeling Curve Resolution. *Organic Process Research & Development* **2020**, *24* (10),

1955-1968.
(42) Ładosz, A.; Kuhnle, C.; Jensen, K. F. Characterization of reaction enthalpy and kinetics in a microscale flow platform. *Reaction Chemistry & Engineering* **2020**, *5* (11), 2115-2122.
(43) Nambiar, A. M. K.; Breen, C. P.; Hart, T.; Kulesza, T.; Jamison, T. F.; Jensen, K. F. Bayesian Optimization of Computer-Proposed Multistep Synthetic Routes on an Automated Robotic Flow Platform. *ACS Central Science* **2022**, *8* (6), 825-836.
(44) Fath, V.; Kockmann, N.; Röder, T. In Situ Reaction Monitoring of Unstable Lithiated Intermediates through Inline FTIR Spectroscopy. **2019**, *42* (10), 2095-2104.
(45) Navid, A.; Khalilarya, S.; Abbasi, M. Diesel engine optimization with multi-objective performance characteristics by non-evolutionary Nelder-Mead algorithm: Sobol sequence and Latin hypercube sampling methods comparison in DoE process. *Fuel* **2018**, *228*, 349-367.
(46) Daulton, S., Balandat, M., Bakshy, E, Parallel bayesian optimization of multiple noisy objectives with expected hypervolume improvement. In *NeurIPS*, 2021; pp 2187-2200.
(47) Luo G, Y. X., Su W, Qi T, Xu Q, Su A. Optimizing telescoped heterogeneous catalysis with noise-resilient multi-objective Bayesian optimization. *ChemRxiv.* **2024**.